Modeling Ion-Exchange for Cesium Removal from Alkaline Radioactive Waste Solutions

F. G. Smith III[a]; L. L. Hamm[a]; S. E. Aleman[a]; M. E. Johnson[b]

[a] Savannah River National Laboratory, Aiken, SC [b] CH2M-HILL Hanford Group, Inc., Richland, WA

PLEASE SCROLL DOWN FOR ARTICLE

Taylor & Francis
Taylor & Francis Group

Modeling Ion-Exchange for Cesium Removal from Alkaline Radioactive Waste Solutions

F. G. Smith III,[1] **L. L. Hamm,**[1] **S. E. Aleman,**[1] **and M. E. Johnson**[2]
[1]Savannah River National Laboratory, Aiken, SC
[2]CH2M-HILL Hanford Group, Inc., Richland, WA

Abstract: The performance of spherical Resorcinol-Formaldehyde ion-exchange resin for treatment of radioactive waste solutions is investigated through computer modeling. Results show that ion-exchange is an efficient method for cesium removal from highly alkaline radioactive waste solutions. On average, two 1300 liter columns operating in series are able to treat 690,000 liters of waste with an initial cesium concentration of 0.09 mM in 11 days achieving a decontamination factor of over 50,000. The study investigated the sensitivity of ion-exchange column performance to variations in flow, temperature, and column dimensions. Modeling results can be used to optimize the design of the ion exchange system.

Keywords: Cesium removal, ion-exchange, process modeling, radioactive waste

INTRODUCTION

Ion-exchange has been investigated as a method for treating liquid radioactive waste for over 50 years (1) because of the high decontamination factors that can be achieved. Radioactive ^{137}Cs is a major contributor to the radioactivity of highly alkaline waste solutions stored at the Savannah River Site in South Carolina and the Hanford Site in Washington state. Cesium removal from these solutions would greatly facilitate further processing. Several ion-exchange media such as zeolites (2) crystalline silico-titinates (3), and resorcinol-formaldehyde (4,5) have

demonstrated high selectivity for cesium removal from radioactive wastes. A review of recent work in this area is provided by the IAEA technical report 408 (6).

A process is currently being designed to remove cesium, containing some isotopic fraction of radioactive ^{137}Cs, from waste solutions at the Hanford site. This process would treat waste solutions with relatively low cesium concentrations to allow processing the treated material as low activity waste. One treatment method being considered is ion-exchange using spherical resorcinol-formaldehyde (RF) resin. RF cation-exchange materials have been demonstrated to efficiently remove cesium from solutions representative of the Hanford site waste compositions (7). RF resin is prepared by condensation polymerization of resorcinol ($C_6H_6O_2$) and formaldehyde (CH_2O). The high selectivity for cesium is attributed to the two weakly acidic hydroxyl groups on resorcinol which ionize and become functional at high pH. Due to its weak acidic nature, the resin has a strong preference for H^+ and can be eluted with dilute nitric acid to remove adsorbed cesium. The cesium-containing eluate would be neutralized and returned to the Hanford site tank farm. The eluted resin would be reused in further ion-exchange cycles. Resorcinol-formaldehyde has been manufactured in crushed or granular form and in a spherical form better suited for column packing.

The proposed design of the ion-exchange process consists of two columns in series (lead column followed by lag column). Each column would have a volume of $1.3 \, m^3$ with a liquid reservoir of equal volume at the head of each column. Figure 1 shows the model representation of the ion-exchange columns with available sampling points numbered 0 through 5. Point 4, at the exit of the lag column, is used as the process control point. When the instantaneous concentration of ^{137}Cs in the effluent of the lag column reaches the low activity waste limit of $15 \, \mu Ci$ per mole of Na the ion-exchange cycle is stopped. Both columns are then flushed with 0.1 M sodium hydroxide and water to remove the residual feed solution and cesium bound to the RF resin would be eluted by running an acidic solution ($\sim 0.5 \, M$) through the column. Eluate containing concentrated cesium would be returned to the Hanford site tank farm for processing as high level waste. The RF ion-exchange columns would be regenerated by treatment with caustic solution and reused until the performance degradation from exposure to chemicals and radioactivity becomes excessive.

The performance of the proposed process has been investigated by modeling the cesium loading phase of the ion-exchange cycle using the VERSE-LC code developed at Purdue University (8). An Excel spreadsheet with Visual Basic coding was used to automatically run a series of VERSE-LC simulations, collect results, and calculate the cumulative

Figure 1. Model representation of ion-exchange process (CSTR - Continuously Stirred Tank Reactor, i.e., a well mixed vessel).

volume of waste processed during each loading cycle and the cesium concentration in the cumulative volume. The modeling assumes that both lead and lag columns are fully eluted after each loading cycle so that no residual cesium remains on the columns and that the columns are fully regenerated after each cycle. We also assume that there is no degradation in column performance due to chemical or radiation exposure. These assumptions imply that all ion-exchange cycles for a particular waste composition and column configuration are identical which simplifies the modeling since only one column loading cycle needs to be calculated for each operating condition and it is assumed that this behavior persists in subsequent cycles.

Cesium adsorption isotherms for RF resin were generated using a detailed thermodynamic model developed at the Savannah River National Laboratory (SRNL) by Aleman and Hamm (9). Parameters in the model were derived from fitting to batch contact data obtained from experiments conducted at SRNL by Nash et al. (10). Ion-exchange column performance was simulated using effective single-component

(cesium) isotherms and column transport models. Based on this methodology, the best estimate column simulations were run for eight feed streams of interest. Sensitivity of the results to variations in column dimensions, flow rate, and operating temperature were investigated for a single feed composition.

We have recently published a brief description of results from a different ion-exchange study (11). In the present paper, we give more details about the calculation methods used and describe model results more completely.

ION-EXCHANGE COLUMN MODELING

Modeling ion-exchange columns requires a model of solute transport through the column and an adsorption isotherm model that specifies the equilibrium relationship between the concentration of ions in solution and those adsorbed on the solid phase. Resin affinity for competing ions has a direct impact on overall column performance. The isotherms shift the breakthrough curve with respect to the number of bed volumes required to reach a specified concentration level and, for nonlinear isotherms, alter the breakthrough curve shape as well as its sensitivity to the inlet feed conditions. The column size and resin mass also have a direct impact on the overall column performance with the particle geometry having slightly less effect. The bed volume may vary over the course of an ion-exchange cycle for resins such as RF that swell and shrink as the solution ionic strength and the pH change. In this study, the bed volume refers to conditions during the loading cycle. Intra-particle mass transport by pore diffusion to available surface sites has a moderate impact on the overall column performance. Increased pore diffusion enhances the rate of mass transfer between the liquid and solid which tends to sharpen the breakthrough curve. Mass transfer by film diffusion across the particle-to-bed boundary and along the column length by axial dispersion have a relatively low impact on overall column performance. Pore diffusion, film diffusion, and axial dispersion all alter the shape of the exit breakthrough curves about the 50% breakthrough concentration level with a slight shifting of the breakthrough curve. Mechanisms such as surface migration or adsorption kinetics are not included in the column model since their impacts were considered to be negligible or are indirectly incorporated into the other features during the parameter estimation process. We assume that kinetics associated with local ion exchange at an active resin surface site are very fast compared to the various liquid mass transfer mechanisms that transport ions to the site.

VERSE-LC solves a set of equations describing one-dimensional transport along the axial dimension of the ion-exchange column coupled to one-dimensional diffusion within a porous particle representing the resin (12). In general, a multi-component model must be used to describe the adsorption of competing species from the liquid phase onto the resin. However, under certain conditions, the multi-component transport equations can be decoupled into a series of single-component transport equations. Reduction to single-component equations is a reasonable approximation when one ion (Cs^+) absorbs onto the resin significantly more than others. The validity of using this approach for the RF system was verified by comparing multi-component (Na^+, K^+, Rb^+, and Cs^+) and single-component (Cs^+) calculations. Very similar results for cesium breakthrough were obtained with both approaches. Sodium breakthrough is the fastest, quickly followed by potassium, somewhat later by rubidium, and an order of magnitude later by cesium. Using the single-component formulation, the cesium breakthrough curve is essentially indistinguishable from that obtained using the four-component model. Since significant time savings are achieved with the single-component model (greater than 500 times faster) and the differences in cesium breakthrough are well within our predictive capabilities, the column analyses presented here were all performed using the single-component modeling approach. Typical run times for single-component simulation of one process were on the order of three to five minutes.

For each ionic species, the transport equation solved by VERSE-LC for the liquid phase concentration (c_b) in the axial direction is:

$$\varepsilon_b \frac{\partial c_b}{\partial t} + \varepsilon_b u \frac{\partial c_b}{\partial z} = \varepsilon_b E_b \frac{\partial^2 c_b}{\partial z^2} - \left(\frac{3}{R_p}\right)(1 - \varepsilon_b)k_f\left(c_b - c_p|_{r=R_p}\right) \qquad (1)$$

with boundary and initial conditions:

$$E_b \frac{\partial c_b}{\partial z}\bigg|_{z=0} = u\big[c_b - c_b^{feed}(t)\big], \quad \varepsilon_b E_b \frac{\partial c_b}{\partial z}\bigg|_{z=1} = 0 \text{ and } c_b = c_b(0, z).$$

From left to right, the four terms in Eq. (1) represent storage, advection, axial dispersion, and liquid film diffusion. The transport equation solved for the ion concentration within the resin pores (c_p) is:

$$\varepsilon_p \frac{\partial c_p}{\partial t} + (1 - \varepsilon_p)\overline{C}_T\left(\frac{\partial q}{\partial c_p}\right)\frac{\partial c_p}{\partial t} = \varepsilon_p D_p \frac{1}{r^2}\frac{\partial}{\partial r}\left[r^2 \frac{\partial c_p}{\partial r}\right] \qquad (2)$$

with boundary and initial conditions:

$$\left.\frac{\partial c_p}{\partial r}\right|_{r=0} = 0, \ \varepsilon_p D_p \left.\frac{\partial c_p}{\partial r}\right|_{r=R_p} = k_f(c_b - c_p) \ \text{and} \ c_p = c_p(0, r).$$

The three terms in Eq. (2) represent storage, surface adsorption and pore diffusion.

Assuming local equilibrium between the pore fluid and neighboring surface sites, a multi-component equilibrium isotherm model for the ion exchange between the pore liquid and the solid phase can be expressed as:

$$q = f\left(\overline{C}_T, c_{p1}, c_{p2}, \cdots, c_{pN}\right) \tag{3}$$

where it is assumed that the solid loading fraction (q) can be explicitly related to the total resin capacity ($\overline{C}_T$) and local ion concentrations in the liquid phase.

CESIUM ISOTHERM MODEL

A thermodynamic model of surface adsorption (not described in this paper) was used to generate cesium isotherm data over a range of concentrations for each feed composition. Simulated isotherm data from the thermodynamic model was then fit to an algebraic isotherm model that could be used in VERSE-LC. The RF isotherms apply only for the loading phase of the RF ion-exchange cycle and the elution phase of the RF ion-exchange cycle is not modeled. The modeling assumes that the rate of ion exchange at a surface site is very fast compared to the rate of diffusion within the pore fluid and mass transfer across the liquid film at the outer boundaries of the particles. In other words, we assume that local equilibrium exists between the pore fluid and its neighboring surface sites. With this assumption, an algebraic expression relating ionic or species concentrations in the pore fluid and on the solid RF resin surface sites (referred to as our "isotherm model") can be developed for use in column simulations. We assume that for each feed composition the total cesium capacity of the ion-exchange resin is independent of ionic strength and solution composition throughout the ion-exchange process.

The most general form of the algebraic isotherm model we have used is the Freundlich/Langmuir Hybrid model:

$$\overline{C}_{pi} = \frac{a_i c_{pi}^{M_{ai}}}{\beta_i + \sum_{i=1}^{5} b_i c_{pi}^{M_{bi}}}. \tag{4}$$

Although this form of adsorption isotherm is not thermodynamically consistent, the additional free parameters (M_{ai} and M_{bi}) enabled a better fit to experimental data at low concentrations. Five adsorbing species Cs^+, Na^+, K^+, H^+ and Rb^+ (i = 1, 2, 3, 4, and 5, respectively) were considered. Experimental data suggests that relative RF resin affinities are: $H^+ > Cs^+ > Rb^+ > K^+ > Na^+$.

The general Freundlich/Langmuir Hybrid model can be converted into an effective single-component cesium isotherm by assuming that hydrogen, potassium, sodium, and rubidium concentrations throughout the column quickly reach equilibrium with the RF resin and thereafter remain constant at their feed concentration levels. The terms for these four components in the denominator of Eq. (4) are then combined into an effective single-component isotherm constant for cesium. This effective beta parameter is dependent upon the potassium, sodium, rubidium, and hydrogen feed concentrations but is constant for a given feed composition. We also divide the numerator and denominator of Eq. (4) by b_1 to simplify the result. In addition, Eq. (4) calculates the resin capacity as mol/L of bed volume whereas the total resin capacity (Q_T) is typically measured as mol/g. We therefore set:

$$\frac{a_1}{b_1} = \rho_b \, \eta_{df} \, Q_T \qquad (5)$$

where ρ_b is the bed density (g-resin/L-BV) and η_{df} is a dimensionless resin degradation factor that can be used to lower the total capacity to account for the effects of chemical or radioactive exposure. The final form of the single-component cesium isotherm is:

$$\overline{C}_{pCs} = \eta_{df} \left[\frac{\rho_b Q_T c_{pCs}^{M_{aCs}}}{\beta_{Cs} + c_{pCs}^{M_{bCs}}} \right]. \qquad (6)$$

Isotherm parameters Q_T, β_{Cs}, M_{aCs}, and M_{bCs} are calculated using a computer code developed at SRNL that fit a thermodynamic model of surface adsorption against experimental data. The experiments (10) used a simulant of the Hanford site tank AP-101 waste plus variations about the nominal tank AP-101 composition for batch contact, batch kinetics, and small column ion-exchange experiments.

Column Properties

Properties associated with an ion-exchange column such as bed density and porosity are inherently column specific. Based on geometrical considerations,

not all densities and porosities are independent. The following expressions place constraints on bed porosities:

$$\varepsilon_t = \varepsilon_b + (1 - \varepsilon_b)\varepsilon_p \tag{7}$$

and densities:

$$\rho_b = \rho_s(1 - \varepsilon_t) = \rho_s(1 - \varepsilon_b)(1 - \varepsilon_p). \tag{8}$$

The bed, pore, and total porosities in Eq. (7) are defined as the following volume fractions:

$$\varepsilon_b = \frac{V_{void} - V_{pore}}{V_b}, \quad \varepsilon_p = \frac{V_{pore}}{V_p}, \quad \varepsilon_t = \frac{V_{void}}{V_b} = \frac{V_b - V_s}{V_b}. \tag{9}$$

A bed porosity of 0.42 was measured for a nominal sample of spherical RF resin. German (13) reports an average porosity of 0.363 for dense packing of uniform hard spheres. Greater packing fractions (smaller bed porosities) can be achieved when multi-sized spheres are employed. As discussed in the following section, the particle size distribution for the spherical RF material was relatively narrow so a void volume somewhat greater than that for uniform hard spheres is reasonable.

Resin Properties

The particle size distribution of spherical RF resin (batch 5E-370/641 manufactured by Microbeads AS of Skedsmokorset, Norway) was characterized in both hydrogen and sodium form at Battelle-Pacific Northwest Division (PNWD) by Fiskum et al. (7) and at SRNL by Adamson et al. (14). For ion-exchange column modeling, the particle size in sodium form is required. The bulk of the particle size distribution fell in the 400 to 600 μm range. PNWD reports an average particle diameter of 452 μm while SRNL measured an average particle diameter of 461 μm in a simulant of AP-101 waste composition. The average of these two values, 457 μm, was taken to be the RF particle diameter. A nominal particle radius of 230 μm was used in the model calculations which falls within the uncertainty of the measured values. The particle density of the RF resin in sodium form was measured as 1.615 g/mL during pilot scale hydraulic testing by Adamson et al. (14).

The actual amount of resin present in the column is a parameter of prime importance with respect to column performance. An estimate of column bed density was derived from the data reported by Nash et al. (10). In that study, the mass of dry RF resin in hydrogen form and the

corresponding bed volume during column loading were measured to obtain a nominal column bed density (ion-exchange material bulk density) of:

$$\rho_b = \frac{m_{resin}}{V_b} = 0.256\,g/ml. \tag{10}$$

The resin mass is multiplied by a factor of 1.25 to convert from hydrogen form to sodium form (10). Using the values presented in the above subsections, the particle void fraction of the resin particles in sodium form becomes:

$$\varepsilon_p = 1 - \rho_b/\rho_s(1 - \varepsilon_b) = 0.658. \tag{11}$$

Spherical RF resin has at least two pKa values and the total ion-exchange capacity is a function of liquid-phase ionic strength and pH. Based on experimental data and modeling studies, the total capacity of RF resin was estimated to be 6.75 mmol/g. At high hydroxide concentrations, the apparent ion-exchange capacity for Cs^+ was approximately 0.7 mmol/g.

Solution Properties

Ion-exchange feed compositions used in this study are listed in Table 1. The density and viscosity of each feed solution were calculated from the composition and temperature using Version 2.0 of the Stream Analyzer^{TM} software from OLI Systems, Inc. Solution densities and viscosities at 25°C are listed in Table 2.

Molecular diffusion coefficients are important in determining key dimensionless numbers (e.g., Schmidt Number, Sc) used in various constitutive law correlations for column transport modeling. They also provide an upper bound for pore diffusion coefficients. Binary diffusion coefficients for dilute solutions of single salt electrolytes can be estimated using the Nernst-Haskell equation (15):

$$D_\pm^\infty = \left(\frac{RT}{F^2}\right)\left[\frac{\frac{1}{z_+} + \frac{1}{z_-}}{\frac{1}{\lambda_+^o} + \frac{1}{\lambda_-^o}}\right]. \tag{12}$$

Limiting ionic conductivities (λ°) at 25°C and infinite dilution for the ions of interest in this study are tabulated in Table 3. Most of the conductivities were calculated using the correlation by Anderko (16):

$$\ln[\lambda^0(T)\eta(T)] = A + B/T. \tag{13}$$

Table 1. Molar concentration of ion-exchange feed solutions for all components >1.0 mM and cesium

	AP-104	AP-102	AP-101	AP-103	AP-105	AP-108	AP-107	AN-104
Na^{+1}	6.00	6.00	6.00	6.00	6.00	6.00	6.00	6.00
Cs^{+1}	5.75×10^{-5}	7.57×10^{-5}	8.98×10^{-5}	7.17×10^{-5}	7.75×10^{-5}	5.82×10^{-5}	2.03×10^{-4}	7.96×10^{-5}
K^{+1}	0.117	0.087	0.147	0.095	0.068	0.174	0.075	0.053
OH^{-1}	1.120	1.410	1.040	0.960	1.260	1.450	0.960	1.740
NO_3^{-1}	2.380	1.890	2.820	1.760	1.740	1.900	2.330	1.450
NO_2^{-1}	0.960	1.450	0.680	1.350	1.560	1.170	0.920	1.150
F^{-1}	0.024	0.002	0.031	0.026	0.005	0.013	0.029	0.013
Cl^{-1}	0.094	0.108	0.055	0.108	0.141	0.094	0.059	0.101
$Al(OH)_4^{-1}$	0.420	0.630	0.300	0.540	0.460	0.570	0.310	0.640
CO_3^{-2}	0.360	0.202	0.405	0.436	0.288	0.367	0.481	0.373
SO_4^{-2}	0.044	0.020	0.075	0.040	0.042	0.032	0.119	0.046
PO_4^{-2}	0.047	0.022	0.043	0.040	0.029	0.013	0.039	0.019
$C_2O_4^{-2}$	0.015	0.000	0.016	0.025	0.000	0.007	0.019	0.005
$Cr(OH)_4^{-1}$	0.00920	0.00840	0.01210	0.00919	0.00476	0.01030	0.01540	0.00373
SiO_4^{-4}	0.00170	0.00126	0.00275	0.00209	0.00126	0.00230	0.00112	0.00220
$C_6H_5O_7$	0.039	0.023	0.023	0.068	0.048	0.033	0.026	0.013
^{137}Cs Ci/L	0.14	0.18	0.21	0.17	0.18	0.14	0.48	0.19

Table 2. Feed solution physical properties at 25°C

Waste	Density (g/mL)	Viscosity (Pa s)	Cs$^+$ D$_\infty$ (cm^2/min)
AP-104	1.240	2.64×10^{-3}	4.27×10^{-4}
AP-102	1.235	2.79×10^{-3}	4.18×10^{-4}
AP-101	1.245	2.54×10^{-3}	4.42×10^{-4}
AP-103	1.236	2.76×10^{-3}	4.00×10^{-4}
AP-105	1.232	2.64×10^{-3}	4.35×10^{-4}
AP-108	1.240	2.88×10^{-3}	7.86×10^{-4}
AP-107	1.241	2.57×10^{-3}	12.83×10^{-4}
AN-104	1.234	3.07×10^{-3}	14.62×10^{-4}

The correlation coefficients A and B are listed in Table 3. In a few instances where the anion was not included in the Anderko correlation, literature values of the ionic conductivity (15,17,18) were used.

Using Eq. (12) and the limiting ionic conductivities provided in Table 3, binary molecular diffusion coefficients for certain single salts within an aqueous phase are computed. To account for fluid property differences between a salt solution and pure water, a correction factor

Table 3. Limiting ionic conductivity fitting coefficients and calculated conductivities in water at 25°C

	A	B	Limiting ionic conductivity Ω^{-1}/eq
Cations			
H$^+$	−3.9726	837.79	351.05
Na^{+1}	−3.3594	75.492	50.27
K^{+1}	−3.5730	254.36	73.97
Cs^{+1}	−3.6512	291.42	77.46
Anions			
OH^{-1}	−3.3346	468.13	192.30
Cl^{-1}	−3.4051	216.03	76.94
NO$_3^{-1}$	−3.6743	277.43	72.22
NO$_2^{-1}$			72.00[b]
F^{-1}			55.40[b]
CO$_3^{-2}$			69.30[b]
SO$_4^{-2}$	−2.9457	90.983	80.08
HPO$_4^{-2}$			75.00[a]
Al(OH)$_4^{-1}$			70.00[a]

[a]Estimated value.
[b]Literature value.

is applied based on the Stokes-Einstein equation (19):

$$\frac{D_{AB}\mu_B}{\kappa T} = \frac{1}{6\pi R_A}. \tag{14}$$

From Eq. (14), the ratio of the dynamic viscosity of pure water (representing conditions at infinite dilution) to that of the salt solution is a correction factor that is applied to the molecular diffusion coefficients computed from Eq. (12) to estimate binary diffusion coefficients in the salt solution.

The dominant binary cation-anion pairs (i.e., cesium paired with individual anions based on the given waste compositions) and their computed binary molecular diffusion coefficients are listed in Table 4 at 25°C. An overall diffusion coefficient for cesium was estimated as the average of the individual cesium pair diffusion coefficients weighted by the mole fraction of each pair in solution. The calculation for the AP-104 waste composition is shown in Table 4. Diffusion coefficients calculated using this method for the feed solutions considered in this study are listed in Table 2.

Particle Kinetics Parameters

The rate of cesium uptake by the RF resin controls the transient behavior of the column. As the rate of cesium uptake by the resin is increased, the

Table 4. Binary molecular diffusion coefficients at 25°C for a solution containing cesium cations and anion of one particular species

Ion Pairs	Molecular diffusion coefficient in water (cm^2/min)	Molecular diffusion coefficient in AP-104 waste (cm^2/min)
Cs^+/OH^{-1}	1.78×10^{-3}	3.61×10^{-4}
Cs^+/Cl^{-1}	1.23×10^{-3}	2.08×10^{-5}
CS^+/NO_3^{-1}	1.19×10^{-3}	5.12×10^{-4}
CS^+/NO_2^{-1}	1.19×10^{-3}	2.07×10^{-4}
Cs^+/F^{-1}	1.03×10^{-3}	4.43×10^{-6}
CS^+/CO_3^{-2}	8.76×10^{-4}	5.72×10^{-5}
CS^+/SO_4^{-2}	9.42×10^{-4}	7.47×10^{-6}
CS^+/PO_4^{-3}	8.11×10^{-4}	6.97×10^{-6}
$CS^+/Al(OH)_4^{-1}$	1.17×10^{-3}	8.94×10^{-5}
$D_\infty\ Cs^+$ (cm^2/min)		1.27×10^{-3}
$D_\infty\ Cs^+$ (cm^2/min) viscosity corrected		4.27×10^{-4}

breakthrough curve becomes sharper and the utilization of the resin is increased. Thus, an accurate evaluation of the parameters that control the rate of cesium uptake is essential for modeling column performance. We assume that the rate of chemical adsorption is very fast when compared to the rates of diffusion within the pore fluid and mass transfer across the liquid film at the outer boundary of the particles. Hence, within the resin particles, the rate of cesium uptake is dominated by intra-particle diffusion. Diffusion within the particles is governed by the pore diffusivity, particle porosity, and the size of the particles. Externally, the rate of cesium transport from the inter-particle fluid to the particle surface depends upon the film mass transfer coefficient. Due to their influence on the rate of cesium uptake and, thus, the transient behavior of the column, the particle porosity, pore diffusivity, particle radius, and the film mass transfer coefficient are referred to as kinetics parameters.

In the VERSE-LC code, the model for intra-particle diffusion assumes that the particles are spheres of uniform radius. To apply the VERSE-LC model it is therefore necessary to determine an average radius from the particle size distribution, as discussed in the section titled "Resin Properties", and an effective pore diffusivity. We assume that the pore sizes are large relative to the size of the migrating ions of interest and that pore diffusion coefficients should not be significantly lower than their bulk or free stream values. However, some level of reduced diffusion in the pores is expected resulting from bends along the pore paths that are generally accounted for by a particle tortuosity factor τ defined as:

$$D_p = \frac{D_\infty}{\tau}. \tag{15}$$

A nominal tortuosity factor of $\tau = 3$ for spherical RF resin was determined by analyzing experimental data obtained at SRNL [20].

Film Diffusion

For laboratory-scale column tests and the proposed full-scale facility, the Reynolds number ranges from approximately 0.1 to one. With respect to published literature values this is a very low Reynolds number range. Numerous mass transfer correlations exist as discussed by Foo and Rice [21]. One of the correlations is that developed by Wilson and Geankoplis [22] based on low Reynolds number data. Large variations between correlations exist; however, the sensitivity of ion-exchange results to the film coefficient has typically been low. VERSE-LC has the Wilson and Geankoplis correlation as an option and this correlation falls somewhat

within the spread of available low Reynolds number data. Therefore, we have used it for the column simulations reported here.

For each ionic species, the Wilson-Geankoplis correlation is:

$$J \equiv \left[\frac{k_{fi}}{u\varepsilon_b}\right] Sc_i^{2/3} = \frac{1.09}{\varepsilon_b} Re^{-2/3}. \tag{16}$$

In Eq. (16), k_{fi} is the film mass transfer coefficient for species i, and the Reynolds number (Re) and Schmidt number (Sc) are defined as:

$$Re \equiv \frac{2R_p\rho_w u\varepsilon_b}{\mu_w} \text{ and } Sc_i \equiv \frac{\mu_w}{\rho_w D_i^\infty}, \text{ respectively.}$$

A standard deviation of approximately 25% is reported for Eq. (16) by Wilson and Geankoplis (22), while from a comparison to the various correlations presented by Foo and Rice (21) a standard deviation of 100% to 200% is actually observed.

Axial Dispersion

Axial dispersion in packed columns is the result of mechanical dispersion added onto molecular diffusion. At practical flow rates mechanical dispersion dominates. For well-packed columns of sufficient diameter such that wall effects (channeling) are minimal, a variety of correlations exist for long column performance.

In the low Reynolds number range of interest, the Chung and Wen (23) correlation is applicable for sufficiently large columns (large diameter and length). The axial dispersion coefficient E_b (cm^2/min) is expressed as:

$$E_b = \frac{2R_p u\varepsilon_b}{0.2 + 0.011Re^{0.48}}. \tag{17}$$

The standard deviation of this correlation based on all available data points was reported to be 46%. Equation (17) applies for sufficiently large columns and correction factors must be considered for columns with small diameters and/or short active bed lengths. A brief discussion of minimum column sizing is given by Brooks (24).

MODEL BENCHMARKING

A model calculation was made simulating a small column experiment that used spherical RF resin (batch 5E-370/641) with actual diluted

AP-101 waste as feed. A full description of the test is reported by Fiskum et al. (7). A comparison of simulation results to experimental data is shown in Figs. 2 and 3. Model parameters used in this simulation were computed using the same methods described in the preceding sections of this report. A complete description of the calculation is given by Aleman et al. (20). Figures 2 and 3 show that the model is in good agreement with the data for both the lead and lag columns even at low cesium concentrations (C_0 for this experiment was 4.48×10^{-5} M). From Fig. 3, we see that the model is able to predict cesium concentrations down to the point at which measurement uncertainty, evidenced by scatter in the data points, becomes significant. Both model and data predict 50% breakthrough in the lead column at approximately 95 bed volumes. The good agreement obtained between the experiment and the calculation for this case provides some validation of the model for the waste feed compositions of interest and gives confidence that the simulation results will be accurate.
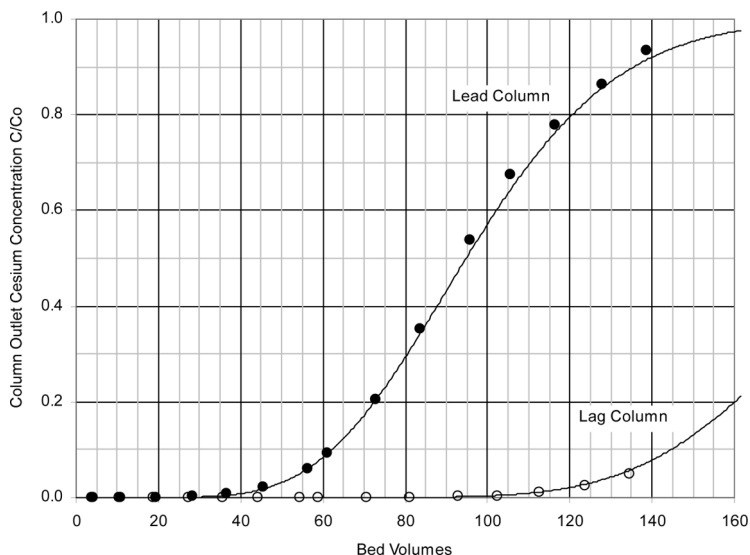

Figure 2. Linear plot of cesium breakthrough predictions compared to data from small column experiment with actual AP-101 waste. Column operating conditions: Flow rate $= 2.89$ BV/h, Temperature $= 26$ to $27°$C, ^{137}Cs $C_0 = 117 \, \mu$Ci/mL, BV in 0.5 M NaOH feed condition $= 11$ mL, Na concentration $= 5.13$ M.
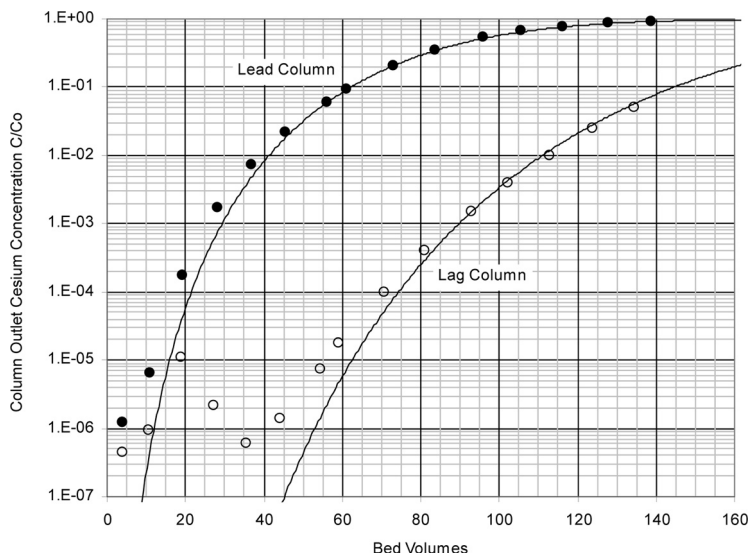
Figure 3. Semi-log plot of cesium breakthrough predictions compared to data from small column experiment with actual AP-101 waste.

COLUMN SIMULATIONS

Ion-exchange processing for the eight waste tank compositions listed in Table 1 was simulated at nominal operating conditions defined to be a bed volume of $1.3\,m^3$ (340 gallons), bed diameter of 0.91 m (36 inches), flow rate of two bed volumes per hour and operating temperature of 25°C. Five additional runs were made using the AP-104 feed composition to test the sensitivity of the results to variations in column size, flow rate and operating temperature in the following combinations:

1. Column diameters of 0.76 and 1.07 m with a flow rate of 2 BV/h at 25°C
2. Flow rates of 1 and 3 BV/h in a 0.91 m diameter column at 25°C
3. A temperature of 15°C in a 0.91 m diameter column with a flow rate of 2 BV/h. In all cases, the column volume was fixed at $1.3\,m^3$.

   Qualitatively results of the sensitivity runs are predictable. The results are expected to be relatively insensitive to changes in the column diameter keeping the bed volume constant. Operation at lower flow will sharpen the breakthrough curve and allow more salt solution to be processed during each cycle at the expense of longer operating time.

Conversely, operation at a higher flow will spread out the breakthrough curve and decrease the amount of salt solution that can be processed during each cycle with some savings in operating time. Operation at lower temperature increases resin capacity by changing the adsorption isotherm.

The simulations assume that both lead and lag columns are fully eluted and regenerated after each loading cycle. We also assume that there is no degradation in column performance due to chemical or radiation exposure. RF-resin will degrade somewhat with each loading cycle (25) but we have not attempted to model this phenomena.

Cesium Isotherms

Experimental batch contact data for cesium on spherical RF resin from Nash et al. (10) was fit to a Freundlich/Langmuir isotherm to more accurately capture the behavior at low cesium concentrations. This same methodology was used to calculate cesium isotherms for the Hanford site waste feed compositions. Table 5 lists the cesium adsorption isotherm parameters used in the VERSE-LC calculations for each feed. The last two columns in Table 5 show the total cesium loading on the RF resin at equilibrium in mol/L of bed volume and the corresponding curies ^{137}Cs/L of bed volume. That is, these values show the cesium loading in a fully loaded column. Since the lead column is typically fully loaded, the curie loadings listed in the last column of Table 5 provide an estimate of the maximum heat load on an ion-exchange column for thermal analysis. The AP-107 waste produces the highest curie loading on the ion-exchange column, 128 Ci/L of bed volume at 25°C. The lowest curie loading is about 36 Ci/L BV for the AP-108 waste. Trends in cesium

Table 5. Cesium adsorption isotherm parameters at 25°C

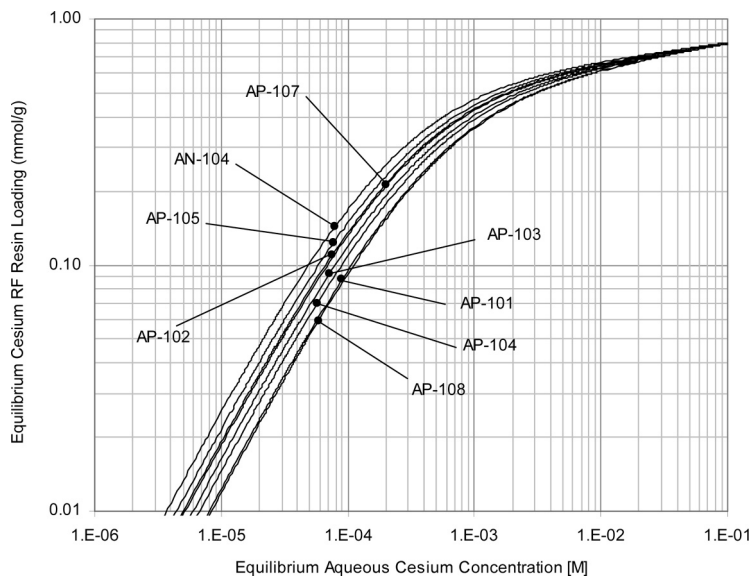| Waste	a	β	M_a	M_b	Cs concentration mol/L	Cs radioactivity Ci/L
AP-104	0.248	8.38×10^{-4}	0.976	0.894	0.0179	43.70
AP-102	0.245	6.37×10^{-4}	0.974	0.899	0.0283	67.30
AP-101	0.250	9.88×10^{-4}	0.978	0.890	0.0223	52.25
AP-103	0.246	7.49×10^{-4}	0.976	0.896	0.0237	56.11
AP-105	0.243	5.67×10^{-4}	0.974	0.901	0.0316	73.38
AP-108	0.252	1.03×10^{-4}	0.978	0.889	0.0151	36.42
AP-107	0.244	6.57×10^{-4}	0.975	0.898	0.0541	127.88
AN-104	0.242	4.79×10^{-4}	0.973	0.904	0.0368	87.88

Figure 4. Cesium adsorption isotherms at nominal operating conditions.

loading generally correlate with feed cesium concentrations given in Table 1 since the waste compositions are similar.

Figure 4 shows cesium adsorption isotherms for the eight waste compositions analyzed. The points on the isotherms in Fig. 4 are plotted at the feed equilibrium aqueous cesium concentration (x-axis) and indicate the cesium concentration on the RF resin (y-axis) at equilibrium with the feed. In general, the higher up the isotherm curve the inlet cesium concentration falls the more nonlinear the shape of the isotherm which tends to sharpen the breakthrough curve. For example, waste composition AP-107 falls higher along its isotherm than any of the other feed compositions and, as shown below, produces the steepest breakthrough curve. However, other factors such as cesium diffusivity also have a significant impact on the shape of the predicted breakthrough curve.

Column Modeling Results

Results from the AP-104 sensitivity runs are summarized in Table 6 and plots of lag column breakthrough curves for the sensitivity runs are presented in Figs. 5 through 7. In Table 6: Case 2 represents the nominal operating conditions, Cases 1 and 3 investigate different column

Table 6. Sensitivity study results

Case	Column diameter (m)	Flow rate (BV/h)	Temperature (C)	AP-104 Volume processed/cycle (m^3)	Loading cycle time (Days)
1	0.76	2	25	582.5	9.41
2	0.91	2	25	579.1	9.35
3	1.07	2	25	575.7	9.30
4	0.91	1	25	669.2	21.61
5	0.91	3	25	512.9	5.52
6	0.91	2	15	777.8	12.57

diameters, Cases 4 and 5 investigate different flow rates, and Case 6 investigates operation at a lower temperature.

As can be seen from Table 6, VERSE-LC results for the three different column diameters are within the uncertainty of the calculation and therefore essentially identical. VERSE-LC is a one-dimensional (axial) model of the column so results will not be very sensitive to changes in column dimensions. Axial dispersion will tend to diffuse the adsorption front slightly more with longer residence times in longer columns.
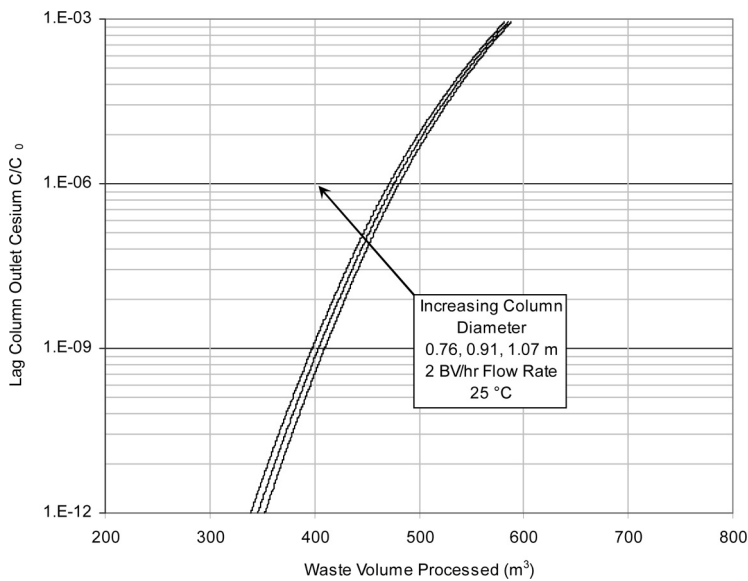

Figure 5. Lag column breakthrough curves for AP-104 waste composition with varying column diameter at nominal flow and temperature.

However, this effect is small. Figure 5 shows the breakthrough curves obtained with varying column diameter where the small difference in results with variation in column dimensions is apparent.

Flow rate does have a significant impact on column performance. Lower flow rates allow more time for diffusion into the ion-exchange particles and equilibration which will sharpen the wave front, retard breakthrough, and make better use of the ion-exchange resin capacity. The results in Table 6 quantify this effect. As shown in Table 6, lowering the flow rate from 2 BV/h (Case 2) to 1 BV/h (Case 4) increases the amount of waste that can be treated in a single ion-exchange cycle by about 16%. However, the loading time is increased by 130%. Increasing the flow rate to 3 BV/h (Case 5) decreases the volume of waste processed by about 11% and decreases the processing time by about 40%. Faster processing times will also reduce RF resin exposure to chemical and radioactive degradation. The results indicate that the relatively small gain in waste volume processed at the lower flow rate is probably not worth the increased loading time and resin exposure. However, faster processing rates will reduce both the operating time and the resin exposure with a relatively small penalty in column usage. Figure 6 shows the breakthrough curves obtained by varying the flow rate through the column.
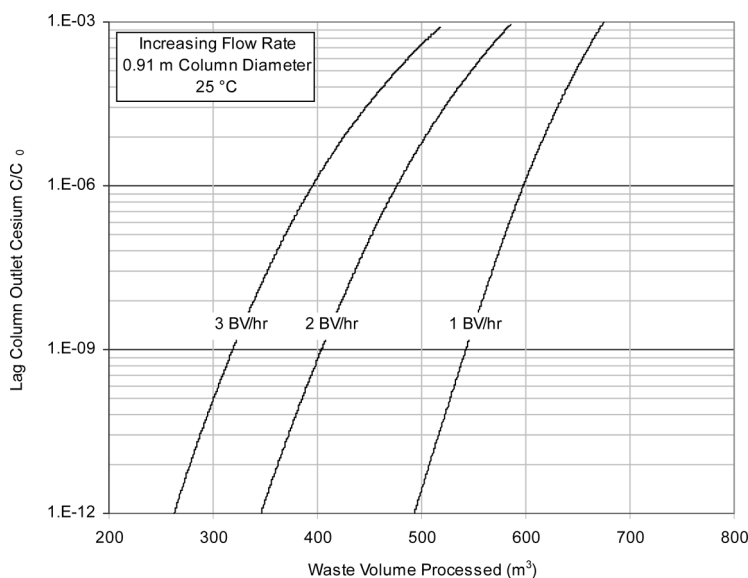

Figure 6. Lag column breakthrough curves for AP-104 waste composition with varying flow rate at nominal column diameter and temperature.

The flow rate is clearly a significant factor in ion-exchange column performance with lower flow increasing column utilization.

Operating the ion-exchange column at 15°C (Case 6) instead of 25°C increases the amount of waste that can be treated in a single cycle by about 34%. The number of loading cycles required to process the AP-104 waste is thereby reduced from 25 to 19. The trade off is the necessity of providing cooling to the ion-exchange column. Some cooling will be required to maintain the ion-exchange column at 25°C since cesium loading on the fully loaded lead column ranges from 40 to 130 Ci/L of bed volume for the given feeds. Heat generation in the fully loaded lead column ranges from approximately 240 to 790 watts. Figure 7 shows the breakthrough curves obtained running the column at 25°C and 15°C with nominal flow rate and the column diameter. Temperature has a significant impact with lower temperature improving ion-exchange column performance. The temperature effect is primarily a function of the change in the cesium adsorption isotherm with temperature.

Table 7 summarizes results obtained for the eight feed compositions operating the ion-exchange column at nominal conditions. The table shows the total volume of each waste solution that must be processed, the volume that can be processed in a single ion-exchange cycle, the time
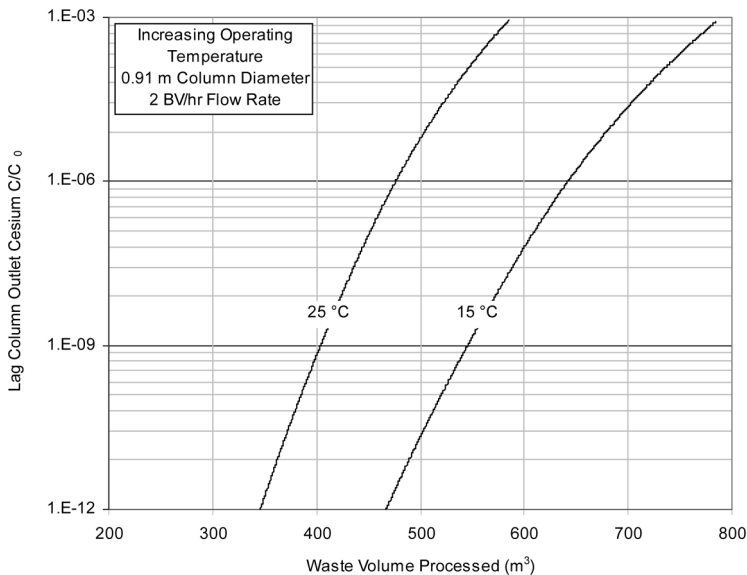
Figure 7. Lag column breakthrough curves for AP-104 waste composition with varying temperature at nominal column diameter and flow rate.

Table 7. Simulation results for feed compositions under nominal operating conditions (0.91 m column, 2 BV/h, 25°C)

Waste	Total waste volume (m^3)	Volume processed/ cycle (m^3)	Loading cycle time (Days)	Number of loading cycles	Total load time (Days)
AP-104	3786.9	582.5	9.35	6.50	60.8
AP-102	4004.2	729.0	11.78	5.49	64.7
AP-101	4126.0	473.9	7.65	8.71	66.6
AP-103	4244.9	620.7	10.03	6.84	68.6
AP-105	3944.0	816.8	13.19	4.83	63.7
AP-108	4336.9	541.6	8.75	8.01	70.1
AP-107	4317.9	648.7	10.48	6.66	69.8
AN-104	5528.0	1112.0	17.96	4.97	89.3

in days required for the loading phase of the cycle, the number of cycles required to process the entire waste volume, and the total loading time required to process the entire waste volume. These estimates assume a clean fresh column for each cycle while it is expected that column performance will degrade over time from exposure of the resin to chemicals and radioactivity. We have also not attempted to include the time required for feed flushing, column elution, column regeneration, and replacement of spent resin although these times are expected to be much shorter than the time required to load the columns, based on laboratory and pilot-scale tests.

The column will be operated until the cesium concentration at the outlet of the lag column is at the limit for processing the decontaminated solution (15 μCi/mole Na). Since the ion-exchange column quickly becomes saturated with sodium we can assume that the sodium concentration in the decontaminated solution is the same as the feed concentration of 6 M. Therefore, the decontaminated solution limit is 90 μCi/L. Cesium activity is relatively constant for all of the feeds having an average value of 2375 Ci/mole [137]Cs. However, total cesium concentrations in the feed solutions vary so individual concentration limits must be set for each feed.

Plots of lag column breakthrough curves for the eight feed compositions are shown in Fig. 8. The volume of waste solution that can be processed during a single ion-exchange cycle varies from about 470 m^3 for AP-101 up to almost 1140 m^3 for AN-104. Table 8 shows the ratio of the cesium concentration in the composite (cumulative) product to the processing limit for each feed composition. Operating the column until the outlet concentration is at the processing limit is very conservative
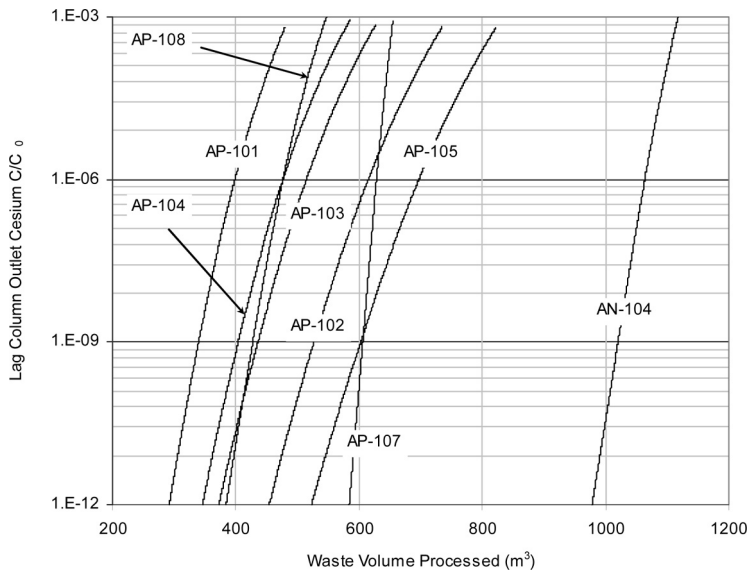
Figure 8. Lag column breakthrough curves for waste compositions under nominal operating conditions.

and the cumulative product compositions are between 30 and 140 times lower than the effective limit of 90 μCi/L. From Fig. 8, we estimate that increasing the product concentration by an order of magnitude might allow an additional 95 m^3 of waste to be treated during each ion-exchange loading cycle.

Table 8. Decontamination factors for feed compositions (0.91 m column, 2 BV/h, 25°C)

Waste	$C_{composite}/C_{limit}$	DF required	DF predicted
AP-104	0.033	1556	47450
AP-102	0.029	2000	68970
AP-101	0.031	2333	75260
AP-103	0.032	1889	59030
AP-105	0.027	2000	74070
AP-108	0.022	1556	70730
AP-107	0.007	5333	772900
AN-104	0.008	2111	261900

Figures 9 through 11 show concentration profiles within the liquid phase in the lag column at the end of the loading cycle for the AP-104 sensitivity runs. The column length (x-axis) is normalized such that 1.0 is the inlet of the lag column and 2.0 is the outlet of the lag column. For the nominal 0.91 m diameter, the actual column length is approximately two meters (1.96 m) while in Fig. 9, the column length varies from 1.44 m for the 1.07 m diameter column to 2.82 m for the 0.76 m column. The sensitivity results show relatively small differences for different column geometries and significant differences for variations in flow rate and temperature. Figure 10 clearly shows the better use of the RF resin capacity obtained at lower flow rates.

Figure 12 shows concentration profiles within the liquid phase in the lag column at the end of the loading cycle for the eight waste feed compositions. The column length is again normalized. Waste compositions AP-107 and AN-104 have particularly steep breakthrough curves so that both the lead and the lag columns are almost completely loaded at the end of a cycle. Review of the calculations showed that this is primarily caused by the relatively high cesium diffusivities predicted for these waste compositions (Table 2). High diffusivity allows the cesium to enter the RF pores faster and equilibrate with the adsorption sites more efficiently.
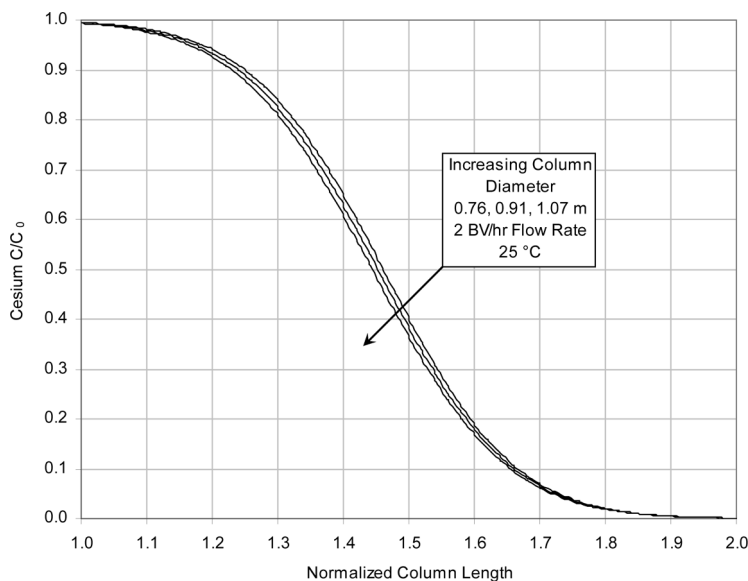
Figure 9. Cesium concentration profiles in lag column at end of loading cycle for AP-104 waste with varying column diameter at nominal flow and temperature.
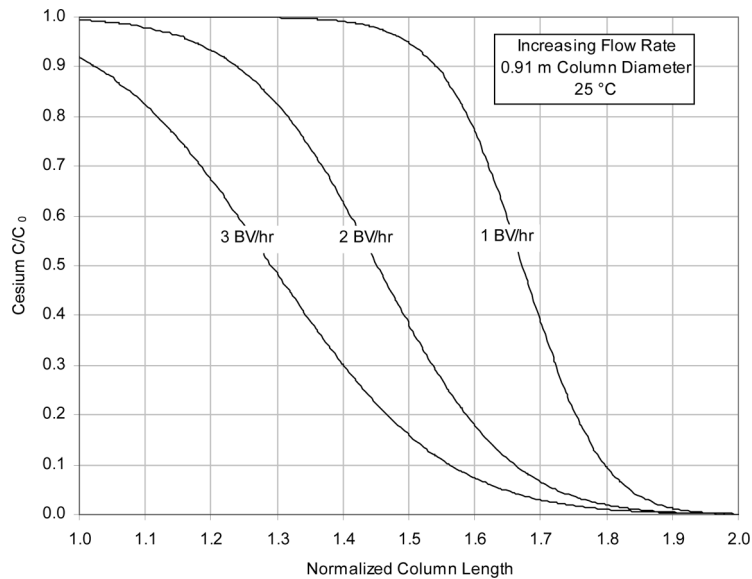
Figure 10. Cesium concentration profiles in lag column at end of loading cycle for AP-104 waste with varying flow rates at nominal column diameter and temperature.
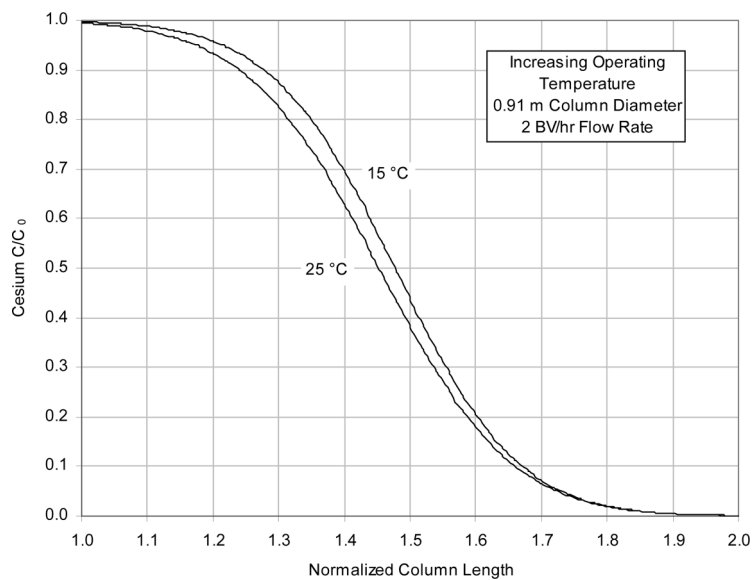

Figure 11. Cesium concentration profiles in lag column at end of loading cycle for AP-104 waste with varying temperature at nominal column diameter and flow rate.
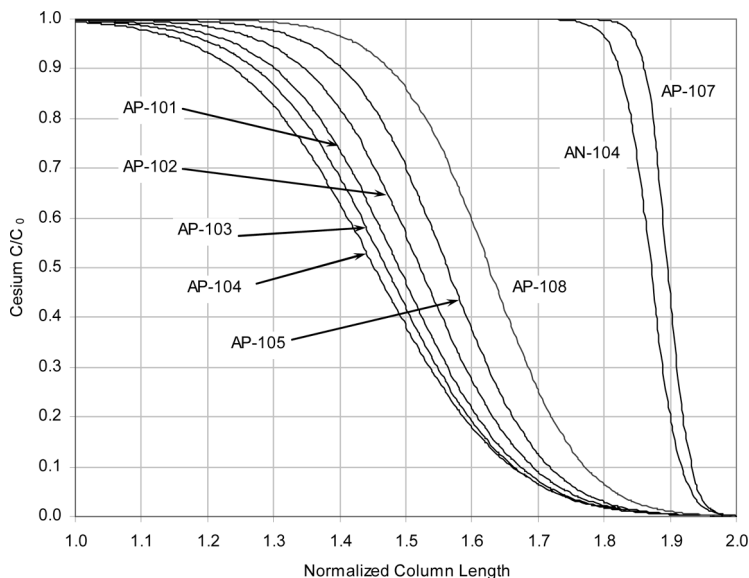
Figure 12. Cesium concentration profiles in lag column at end of loading cycle for waste compositions at nominal operating conditions.

CONCLUSIONS

The VERSE-LC code has been used to determine the performance of spherical Resorcinol-Formaldehyde (RF) ion-exchange resin for the removal of cesium from eight Hanford waste solutions. In all cases, the RF resin was predicted to process a significant volume of waste solution during each ion-exchange cycle. Sensitivity analysis shows that lower flow sharpens the breakthrough front which makes fuller use of the resin capacity allowing more waste volume to be processed in each ion-exchange cycle. However, decreasing the flow from 2 BV/h to 1 BV/h increases the volume of the solution processed in each loading cycle by about 16% while also increasing the time required to run a loading cycle by 130%. Hence, there is a significant penalty in longer operating time for a modest increase in capacity.

The calculations also show that higher flow spreads out the breakthrough front and decreases the amount of solution that can be processed in each ion-exchange cycle. Increasing the flow from 2 BV/h to 3 BV/h decreases the volume of solution processed by about 11% while decreasing the time required to run the material through the column by about 60%. However, using higher flow rates is attractive since the operating

times are substantially decreased with only a modest penalty in column capacity. Processing at a higher flow would also decrease the exposure of the RF resin to radiolytic degradation thereby increasing the volume of waste that each bed can process before it must be replaced.

Operating the column at a lower temperature increases the adsorption capacity of the resin and increases the amount of solution that can be treated in each cycle. Operating at 15°C instead of 25°C increased RF resin capacity by approximately 34%. However, unless the feeds are naturally chilled (e.g., as a result of below ground storage), the need to supply active cooling to the column will increase equipment costs offsetting some of the savings from an increase in capacity. Column performance was insensitive to variations in column geometry over a practical range of design options.

While the model of solute transport through the ion exchange column applied in this study is not new, we have demonstrated a methodology to obtain accurate input parameters for application of the model to the simulation of radioactive waste treatment. In particular, experimental data was used to derive an appropriate isotherm model, the model of column performance was benchmarked against experimental data, and sensitivity studies were made with the model to guide process design.

NOMENCLATURE

A, B	conductivity correlation coefficients
a_i, b_i	isotherm coefficients for species i
c_b	concentration in bed fluid, M
c_p	concentration in pore fluid, M
C_0	concentration in feed solution, M
$\overline{C}_{pi}$	concentration of species i on solid based on bed volume, mol/L-BV
$\overline{C}_T$	total ion-exchange capacity of resin, mol/L-BV
D_{AB}	binary diffusion coefficient for chemical species A in solution B, cm^2/min
D_p	pore diffusivity of Cs$^+$ in the particle pore, cm^2/min
D_∞	bulk diffusivity of Cs$^+$ in the free stream, cm^2/min
$D_\pm^\infty$	binary diffusion coefficient at infinite dilution, cm^2/min
D_i^∞	diffusion coefficient for species i at infinite dilution, cm^2/min
E_b	axial diffusion coefficient, cm^2/min
F	Faraday constant, 96500 C/eq
DF	Decontamination Factor, ratio of influent to effluent cesium concentrations

k_f	liquid film mass transfer coefficient, cm/min
M_{ai}, M_{bi}	isotherm exponents for species i
q	species fractional loading on resin
Q_T	total resin capacity, mol/g
r	radial coordinate within resin particle, cm
R	gas constant, $8.314\,J\,mol^{-1}\,K^{-1}$
R_A	radius of diffusing particle, cm
R_p	average particle radius, cm
t	time, min
T	absolute temperature, K
u	interstitial fluid velocity, cm/min
V_b	total volume of bed, mL
V_{void}	total volume of voids within bed, mL
V_{pore}	total volume of pores within particles, mL
V_p	total volume of particles within bed, mL
V_s	total volume of solid resin within bed, mL
z	axial coordinate, cm
z_+, z_-	valences of cation and anion, respectively

Greek Symbols

β_i	isotherm coefficient for species i
ε_b	bed porosity
ε_p	particle porosity
ε_t	total porosity of bed
κ	Boltzmann constant
λ_+^o, λ_-^o	limiting ionic conductivity for cation and anion, $\Omega^{-1}\cdot cm^2/eq$
η_{df}	resin degradation fraction
μ_B	dynamic viscosity of solution
μ_w	dynamic viscosity of water
$\eta(T)$	viscosity of pure water, $Pa\cdot s$
ρ_b	bed density, g/mL
ρ_s	solid density of resin, g/mL
ρ_w	density of water, g/mL
τ	tortuosity factor

Subscripts

i	ionic species
b	bed
p	particle
s	solid
t	total

REFERENCES

1. Ayers, J.A. (1951) Treatment of radioactive waste by ion exchange. *Ind. & Eng. Chem.*, *43* (7): 1526–1531.

2. Sinha, P.K.; Panicker, P.K.; Amalraj, R.V.; Krishnasamy, V. (1995) Treatment of radioactive liquid waste containing caesium by indigenously available synthetic zeolites: A comparitive study. *Waste Manage.*, *15*: 149–157.

3. Anthony, R.G.; Philip, C.V.; Dosh, R.G. (1993) Selective adsorption and ion exchange of metal cations and anions with silico-titinates and layered titinates. *Waste Manage.*, *13*: 503–512.

4. Samanta, S.K.; Ramaswamy, M.; Misra, B.M. (1992) Studies on cesium uptake by phenolic resin. *Sep. Sci. Technol.*, *27*: 255–267.

5. Samanta, S.K.; Theyyunni, T.K.; Misra, B.M. (1994) Column behavior of resorcinol-formaldehyde polycondensate resin for radiocesium removal from simulated radwaste solution. *J. Nuc. Sci. Technol.*, *32* (5): 425–429.

6. International Atomic Energy Agency (IAEA). (2002) Application of ion exchange processes for the treatment of radioactive waste and management of spent ion exchangers. *Tech.* Report Series No. 408, Vienna.

7. Fiskum, S.K.; Arm, S.T.; Fountain, M.S.; Steele, M.J.; Blanchard, D.L. (2006) "Spherical Recorcinol-Formaldehyde Resin Testing for ^{137}Cs Removal from Simulated and Actual Hanford Waste Tank 241-AP-101 Diluted Feed (Envelope A) Using Small Column Ion Exchange," WTP-RPT-134, Battelle-Pacific Northwest: Richland, WA.

8. Whitley, R.D.; Wang, N.-H.L. (1998) *User's Manual VERSE (VErsatile Reaction SEparation) Simulation for Liquid Phase Adsorption and Chromatography Processes*; School of Chemical Engineering, Purdue University.

9. Aleman, S.E.; Hamm, L.L. (2007). *Detailed Thermodynamic Equilibrium Model for the Prediction of Ion Exchange Behavior on Monovalent Cation Exchange Resins*; WSRC-STI-2007-00054, Washington Savannah River Co.: Aiken, SC.

10. Nash, C.A.; Duignan, M.R.; Duffey, C.E. (2006) *Batch, Kinetics, and Column Data from Spherical Resorcinol-Formaldehyde Resin*; WSRC-STI-2006-00071, Washington Savannah River Co.: Aiken, SC.

11. Smith, F.G.; Lee, S.-Y.; King, W.D.; McCabe, D.J. (2008) Comparisons of crystalline silicotitanate and resorcinol formaldehyde media for cesium removal by in-tank column processing. *Sep. Sci. and Technol.*, *43* (9): 2929–2942.

12. Berninger, J.; Whitley, R.D.; Zhang, X.; Wang, N.-H.L. (1991) A versatile model for simulation of reaction and nonequilibrium dynamics in multicomponent fixed-bed adsorption processes. *Comp. Chem. Eng.*, *15* (11): 749–768.

13. German, R.M. (1989) *Particle Packing Characteristics*; Metal Powder Industries Federation: , Princeton, New Jersey.

14. Adamson, D.J.; Fowley, M.D.; Steimke, J.L.; Steeper, T.J.; Williams, M.; Duffey, C.E.; Fondeur, F.F. (2006) *Pilot-Scale Hydraulic Testing of Resorcinol Formaldehyde Ion Exchange Resin*; WSRC-TR-2005-00570, Washington Savannah River Co.: Aiken, SC.

15. Reid, R.C.; Prausnitz, J.M.; Sherwood, T.K. (1977) *The Properties of Gases and Liquids;* 3rd Ed.; McGraw-Hill Chemical Engineering Series, McGraw-Hill Book Company, Inc.

16. Anderko, A.; Lencka, M.M. (1997) Computation of electrical conductivity of multicomponent aqueous systems in wide concentration and temperature ranges. *Ind. Eng. Chem. Res.*, *36*: 1932–1943.

17. Perry, R.H.; Chilton, C.H., Kirkpatrick, S.D. (Eds.). (1973) *Chemical Engineer's Handbook;* 5th Ed.; McGraw-Hill.

18. Glasstone, S.; Lewis, D. (1960) *Elements of Physical Chemistry*; D. Van Nostrand Company, Inc.: Princeton, N.J.

19. Bird, R.B.; Stewart, W.E.; Lightfoot, E.N. (1960) *Transport Phenomena*; John Wiley and Sons, Inc.: New York.

20. Aleman, S.E.; Hamm, L.L.; Smith, F.G. (2007) *Ion Exchange Modeling of Cesium Removal from Hanford Waste Using Spherical Resorcinol-Formaldehyde Resin*; WSRC-STI-2007-00030, Washington Savannah River Co.: Aiken, SC.

21. Foo, S.C.; Rice, R.G. (1975) On the predication of ultimate separation in parametric pumps. *AIChE J.*, *21* (6): 1149–1158.

22. Wilson, E.J.; Geankoplis, C.J. (1966) Liquid mass transfer at very low Reynolds numbers in packed beds. *Ind. Eng. Chem. Fund.*, *5* (1): 9–14.

23. Chung, S.F.; Wen, C.Y. (1968) Longitudinal dispersion of liquid flowing through fixed and fluidized beds. *AIChE J.*, *14* (6): 857–866.

24. Brooks, K.P. (1994) *Cesium Ion Exchange using Actual Waste: Column Size Considerations*; TWRSPP-94-091, Battelle-Pacific Northwest: Richland, WA.

25. Duffey, C.E.; Walker, D.D. (2005) *Radiolytic, thermal, and physical degradation testing of spherical resorcinol-formaldehyde resin.* WSRC-TR-2005-00075, Washington Savannah River Co.: Aiken, SC.